

THE BRIGHT SHARC SURVEY: THE CLUSTER CATALOG¹

A. K. ROMER², R. C. NICHOL^{3,4}

Dept. of Physics, Carnegie Mellon University, 5000. Forbes Ave., Pittsburgh, PA-15213. (romer@cmu.edu, nichol@cmu.edu)

B. P. HOLDEN^{2,3}

Dept. of Astronomy and Astrophysics, University of Chicago, 5640 S. Ellis Ave., Chicago, IL-60637. (holden@oddjob.uchicago.edu)

M. P. ULMER & R.A. PILDIS

Dept. of Physics and Astronomy, Northwestern University, 2131 N. Sheridan Rd., Evanston, IL-60207. (ulmer@ossenu.astro.nwu.edu)

A. J. MERRELLI²

Dept. of Physics, Carnegie Mellon University, 5000. Forbes Ave., Pittsburgh, PA-15213. (merrelli@andrew.cmu.edu)

C. ADAMI^{4,5}

Dept. of Physics and Astronomy, Northwestern University, 2131 N. Sheridan Rd., Evanston, IL-60207. (adami@lilith.astro.nwu.edu)

D. J. BURKE^{3,6} & C. A. COLLINS³

Astrophysics Research Institute, Liverpool John Moores University, Twelve Quays House, Egerton Wharf, Birkenhead, L41 1LD, UK. (burke@ifa.hawaii.edu & cac@astro.livjm.ac.uk)

A. J. METEVIER

UCO/Lick Observatory, University of California, Santa Cruz, CA 95064 (anne@ucolick.org)

R. G. KRON

Dept. of Astronomy and Astrophysics, University of Chicago, 5640 S. Ellis Ave., Chicago, IL-60637. (rich@oddjob.uchicago.edu)

K. COMMONS²

Dept. of Physics and Astronomy, Northwestern University, 2131 N. Sheridan Rd., Evanston, IL-60207. (commons@lilith.astro.nwu.edu)

Received 1999 April 12; accepted 1999 August 23rd

ABSTRACT

We present the Bright SHARC (Serendipitous High-Redshift Archival ROSAT Cluster) Survey, which is an objective search for serendipitously detected extended X-ray sources in 460 deep ROSAT PSPC pointings. The Bright SHARC Survey covers an area of 178.6 deg² and has yielded 374 extended sources. We discuss the X-ray data reduction, the candidate selection and present results from our on-going optical follow-up campaign. The optical follow-up concentrates on the brightest 94 of the 374 extended sources and is now 97% complete. We have identified thirty-seven clusters of galaxies, for which we present redshifts and luminosities. The clusters span a redshift range of $0.0696 < z < 0.83$ and a luminosity range of $0.065 < L_x < 8.3 \times 10^{44}$ erg s⁻¹ [0.5-2.0 keV] (assuming $H_0 = 50$ km s⁻¹ Mpc⁻¹ and $q_0 = 0.5$). Twelve of the clusters have redshifts greater than $z=0.3$, eight of which are at luminosities brighter than $L_x = 3 \times 10^{44}$ erg s⁻¹. Seventeen of the 37 optically confirmed Bright SHARC clusters have not been listed in any previously published catalog. We also report the discovery of three candidate “fossil groups” of the kind proposed by Ponman *et al.* (1994).

Subject headings: catalogs — galaxies: clusters: general — galaxies: distances and redshifts — surveys — X-rays: galaxies

1. INTRODUCTION

Clusters of galaxies play a key role in constraining cosmological models. It has been shown (*e.g.* Oukbir & Blanchard 1992; Carlberg *et al.* 1997; Henry *et al.* 1997; Sadat *et al.* 1998; Viana & Liddle 1999) that measurements of the cluster number density, and its evolution, play an important role in the derivation of the mean mass density of the Universe, Ω_m . At present, there is a large disper-

sion in the values of Ω_m derived from measurements of the cluster number density; *e.g.* $\Omega_m = 0.2_{-0.1}^{+0.3}$ (Bahcall & Fan 1998), $\Omega_m = 0.4_{-0.2}^{+0.3}$ (Borgani *et al.* 1999), $\Omega_m = 0.5 \pm 0.14$ (Henry *et al.* 1997), $\Omega_m = 0.85 \pm 0.2$ (Sadat *et al.* 1998), $\Omega_m = 0.96_{-0.32}^{+0.36}$ (Reichart *et al.* 1999).

To fully exploit clusters as cosmological tools one needs to have access to large, objectively selected, cluster cata-

¹Based on data taken at the European Southern Observatory, Kitt Peak National Observatory, Cerro Tololo Interamerican Observatory, Canada France Hawaii & Apache Point Observatory

²Visiting Astronomer, Kitt Peak National Observatory. KPNO is operated by AURA, Inc. under contract to the National Science Foundation.

³Visiting Astronomer, European Southern Observatory.

⁴Visiting Astronomer, Canada France Hawaii Telescope.

⁵Also affiliated with: Laboratoire d'Astronomie Spatiale, Traverse du Siphon, 13012 Marseille, France.

⁶Current address: Institute for Astronomy, Univ. of Hawaii, 2680 Woodlawn Drive, Honolulu, HI 96822.

logs which cover a wide redshift range. Most cluster catalogs constructed prior to 1990 had a very limited redshift range and were not constructed in an objective manner (*e.g.* Abell 1958; Abell, Corwin & Olowin 1989). However, recent developments, such as CCD mosaic cameras, optical plate digitizers and imaging X-ray satellites, have resulted in a growing number of high quality cluster catalogs. These include optically selected cluster samples derived from digitized plate material, *e.g.* the EDCC (Lumsden *et al.* 1992) and the APM (Dalton *et al.* 1994), or from CCD imaging surveys, *e.g.* the PDCS (Postman *et al.* 1996) & the ESO Imaging Survey (Lobo *et al.* 1998). X-ray selected cluster samples derived from imaging X-ray satellite data include those from the Einstein mission, *e.g.* the EMSS cluster sample (Gioia *et al.* 1990), and those from the ROSAT (Truemper *et al.* 1993) mission.

The various ROSAT cluster catalogs divide into two categories; those based on ROSAT All-Sky Survey (RASS) data and those based on ROSAT pointing data. The former category includes the SRCS (Romer 1995), XBACS (Ebeling *et al.* 1996), BCS (Ebeling *et al.* 1998), REFLEX (Bohringer *et al.* 1998; De Grandi *et al.* 1999a) and NEP (Gioia *et al.* 1999; Henry 1997) surveys. Examples of surveys based on ROSAT pointing data are the SHARC (Collins *et al.* 1997); RIXOS (Castander *et al.* 1995); RDCS (Rosati *et al.* 1998); WARPS (Jones *et al.* 1998) and 160deg² (Vikhlinin *et al.* 1998a) surveys. The ROSAT instrument of choice for cluster surveys has been the PSPC, which combines imaging capabilities with a large field of view (2° in diameter), low background contamination and some spectral resolution. The angular resolution of the ROSAT PSPC is better than that of Einstein, allowing one to take advantage of the extended nature of cluster emission to distinguish clusters from X-ray point sources, *e.g.* AGN and quasars. Moreover, the enhanced sensitivity of ROSAT over Einstein means that ROSAT cluster surveys can reach fainter flux limits than the EMSS.

The RASS surveys have yielded several important insights into the clustering properties (Romer *et al.* 1994) and evolution (Ebeling *et al.* 1997; De Grandi *et al.* 1999b) of the $z < 0.3$ cluster population. At higher redshifts, the ROSAT pointing data surveys have shown that there is no evidence for evolution in the cluster population at luminosities fainter than $L_x = 5 \times 10^{44}$ erg s⁻¹ [0.5-2.0 keV] and redshifts less than $z \simeq 0.7$ (Nichol *et al.* 1997; Burke *et al.* 1997; Collins *et al.* 1997; Vikhlinin *et al.* 1998b; Rosati *et al.* 1998; Jones *et al.* 1998; Nichol *et al.* 1999). At brighter luminosities, the 160deg² and Bright SHARC surveys, have provided evidence for negative evolution (Nichol *et al.* 1999; Vikhlinin *et al.* 1998b) similar to that seen in the EMSS cluster sample (Henry *et al.* 1992; Reichart *et al.* 1999).

The SHARC (Serendipitous High-Redshift Archival ROSAT Cluster) survey was designed to optimize studies of X-ray cluster evolution and combines two complementary surveys; a narrow area deep survey and a wide area shallow survey. The former, known as the Southern SHARC, has been described elsewhere, (Collins *et al.* 1997; Burke *et al.* 1997). We introduce the latter survey, the Bright SHARC, here. Unlike the Southern SHARC, the philosophy of the Bright SHARC has been to achieve maximum areal coverage rather than maximum sensitiv-

ity. The Bright SHARC survey covers a total area of 178.6 deg² and has yielded a catalog of 37 clusters with fluxes $\geq 1.63 \times 10^{-13}$ erg s⁻¹ cm⁻². In contrast, the Southern SHARC survey covers only 17.7 deg², but has yielded a similar number of clusters (36) with fluxes $\geq 4.66 \times 10^{-14}$ erg s⁻¹ cm⁻².

We describe below the reduction of the 460 ROSAT PSPC pointings in the Bright SHARC survey (§2), our source detection methodology (§3) and the selection and optical follow-up of cluster candidates (§4 & §5). In sections §6 and §7 we present and discuss the Bright SHARC cluster catalog. Throughout this paper we use $H_0 = 50$ km s⁻¹ Mpc⁻¹ and $q_0 = 0.5$ and define f_{-13} and L_{44} to be the unabsorbed flux (observer frame) and luminosity (rest frame) in the [0.5-2.0 keV] energy band in units of 10^{-13} erg s⁻¹ cm⁻² and 10^{44} erg s⁻¹, respectively.

2. TRANSFER AND REDUCTION OF ROSAT PSPC POINTING DATA

The pointed PSPC data used in the construction of the Bright SHARC was obtained from the HEASARC ROSAT data archive using an automated FTP process over a period of two years starting in June 1995. The criteria used to select data from the archive were: *i*) a listed exposure time greater than 10ksecs and *ii*) an absolute Galactic latitude greater than 20 degrees. Based on these criteria, 638 PSPC pointings were transferred to local machines and then reduced using a pipeline processing based on the Extended Source Analysis Software (ESAS) package (Snowden *et al.* 1994).

An overview of our pipeline is as follows. First, the raw data were sorted into good and bad time intervals. Bad intervals were defined as those in which the background level was higher than 170 counts s⁻¹. Data obtained during bad intervals were discarded. The remaining data were binned, as a function of position, into seven different energy bands –which Snowden *et al.* (1994) define as R1 through R7– to produce seven 512 × 512 pixel maps with a pixel scale of 14".947. The 5 highest energy bands, R3 through R7, were then co-added to produce a hard band [0.4-2.0 keV] count rate map for each pointing. Accompanying each count rate map was a count rate uncertainty map and a vignetting corrected exposure map.

For each of the 638 pointings reduced by the ESAS pipeline, the ROSAT pointing name (column 1), the J2000 position (columns 2 & 3), Galactic latitude in degrees (b , column 4), the exposure time in seconds (column 5) and pointing target (column 6) are listed in appendices A & B. Appendix A lists the 460 pointings selected to form the Bright SHARC survey. Two points should be noted about these 460 pointings. First, 371 of the pointings, those with 3 character extensions *e.g.* ‘n00’, ‘a01’ *etc.*, were processed after an important change was made to the Standard Analysis Software System (SASS). This change effected those pointings for which the total exposure time was broken up into more than one observation interval. After the change, each observation interval was analyzed separately, whereas before the change they were analyzed together. Of these 371 pointings, only 45 have more than one observing interval. For simplicity we decided to include only the longest observing interval in our analysis. Second, the Bright SHARC survey does not include the central 2.5 radius region of PSPC (see §4). This means that we were able to

include several pointings in the survey which had intrinsically extended central targets, *e.g.* galaxies and clusters – as long as those targets did not extend beyond $2'.5$. We discuss cases where Bright SHARC clusters are detected in pointings with cluster targets in Table 2 (see §6) and §7.2.

The 178 pointings listed in appendix B were not included in the Bright SHARC because either an extended X-ray (or optical) source covers most of the field of view, or the pointing is within $< 6^\circ$ of the Magellanic clouds. Extended X-ray and optical objects include low redshift Abell clusters and Galactic globular clusters. The pointings listed in Appendix B were removed after visual inspections of the reduced X-ray data and the Digitized Sky Survey. Despite its subjective nature, this procedure does not undermine the serendipitous nature of the SHARC survey, since it was performed before the cluster candidate list was constructed. We have indicated in column 7 of appendix B why each pointing was rejected from the survey.

3. SOURCE DETECTION

Our source detection algorithm was based on wavelet-transforms (Slezak *et al.* 1990). For our purposes, we required a detection algorithm which (i) was sensitive to both extended and point-like sources, (ii) worked in crowded fields and (iii) took into account a varying background level. Moreover, we wanted our method to be as simple as possible, so that we could define our selection function *a posteriori* using simulations. With these concerns in mind, we chose to convolve the PSPC count rate maps with a spherically symmetric, “Mexican-hat” wavelet. This wavelet, in one dimension, is given by:

$$w(x) = \left(1 - \frac{x^2}{a^2}\right) e^{-\frac{x^2}{2a^2}}, \quad (1)$$

and is the second derivative of a Gaussian (Slezak *et al.* 1990) of width $\sigma = a$. The radially averaged point-spread function of the ROSAT PSPC can be approximated to a Gaussian (Hasinger *et al.* 1992), so this wavelet is well suited to the detection of sources in PSPC images. An additional attraction of this wavelet is that it can be used to determine the extent of a source, since it has a width of $2 \times a$ at its zero-crossing points. A wavelet transform of a PSPC count rate map will, therefore, produce a wavelet coefficient map in which all the sources are bounded by a ring of zero values. The diameter of these zero crossing rings provides a direct measure of the source’s extent in wavelet space.

Ideally, “ a ” should be scaled logarithmically to provide statistically independent wavelet images over the whole range of real and k -space. For any given source, the wavelet coefficient will have a maximum when the value of “ a ” matches the sigma of the best fit Gaussian. However, the use of multiple wavelets would make *a posteriori* simulations of the selection function very complex and CPU intensive. We therefore decided to use only one wavelet convolution ($a = 3$ pixels or $45''$) in our source detection pipeline. This particular wavelet was found, empirically, to be the best compromise between smaller wavelets, which tended to fragment extended sources, and larger wavelets, which tended to blend neighboring sources. The penalty for this simplification was the inclusion of some blended

sources in our extended candidate list (§5) and underestimated cluster count rates (§6.1).

Sources were identified in the wavelet coefficient map by selecting pixels with coefficients above a given threshold. This threshold was set, empirically, to be 7 sigma above the peak of the coefficient distribution. The thresholding technique only highlights the cores of each source, since that is where the wavelet coefficients are highest, so a “friends-of-friends” analysis was run to identify other associated pixels. This was done by growing the sources outwards in the wavelet coefficient map until they reached the zero crossing ring. Once the source boundaries were defined, best fit centroids and ellipses were computed. A filling factor was also derived for each source. This was defined as ratio of the area within the fitted ellipse to the area within the zero-crossing boundary. For $f = 1$, the ellipse fits the source shape exactly, while $f \gg 1$ indicates the presence of blended sources (dumb-bell shapes) or percolation runaways (filamentary shapes).

In total, 10,277 sources were detected in the 460 pointings. To keep track of all of these sources, and their boundaries, a mask file was generated for each pointing so that pixels associated with sources could be distinguished from those that were not. For each source, a 51×51 pixel box, with the source at its center, was extracted from the count rate map. An average background for the box was calculated using all pixels not flagged as belonging to sources. The count rate for the central source was then derived by subtracting this background (appropriately scaled) from the sum of the pixels enclosed by the source boundary. We used this method because it was easy to apply to the thousands of sources detected in the Bright SHARC Survey. (We will refer to the count rates derived in this manner as “wavelet count rates”, cr_W , hereafter.) However, the method has the disadvantage of underestimating the true count rate if the source is extended beyond the wavelet boundary (in §6.1 we describe an alternative method used to derive count rates for known clusters). An approximate signal-to-noise value for each source was also calculated using the count rate uncertainty maps produced by ESAS. It should be noted that certain pixels, those which received less than half the exposure time of the central pixel in the count rate maps, were not included in the “friends-of-friends” analysis. Such pixels included those in the shadow of the PSPC window support structure and those at the edge of the field of view. These regions, which are noisier than those that were well exposed, were not used to define source centers, shapes or wavelet count rates.

4. SELECTION OF CLUSTER CANDIDATES

The majority of X-ray sources can be considered point like in their spatial properties, *e.g.* stars and AGN. In the minority are objects with complex and extended X-ray profiles, such as supernova remnants, galaxies and clusters of galaxies. Of these, only clusters are large enough and bright enough to be detected as extended beyond $z \simeq 0.1$. Therefore the strategy adopted by the SHARC has been to search for clusters only among those ROSAT sources that have a significant extent. This reduces the required optical follow-up significantly. The disadvantage of this approach, however, is that some clusters, *e.g.* those with compact surface brightness distributions, may be excluded from the survey.

Bright SHARC Cluster candidates were selected from the 10,277 sources found in the survey using the following six criteria: The source had to (i) have a signal-to-noise ratio greater than 8, (ii) its centroid had to fall within 90 pixels (22'.4) of the pointing center, (iii) its centroid had to fall more than 10 pixels (2'.5) from the pointing center, (iv) its filling factor had to be less than $f = 1.3$, (v) it had to be more than 3σ extended and (vi) it had to have a count rate higher than $0.01163 \text{ counts s}^{-1}$. The imposition of these criteria cut down the source list from 10,277 (total) to 3,334 (criterion i) to 1,706 (criterion ii) to 374 (criteria iii to v) to 94 (criterion vi). Criterion (i) was imposed because it has been shown (Wirth & Bershad, in preparation) that extent measures can only be derived with confidence for sources meeting a minimum signal-to-noise threshold. Criterion (iii) was applied to avoid including the intended target of the pointing in the candidate list. Criterion (iv) was set empirically with the aim of reducing the number of blended sources and percolation runaways in the candidate list. The rationale for the other criteria is provided below.

The point-spread function of the PSPC degrades significantly as one moves out from the center of the detector (Hasinger *et al.* 1992). It therefore becomes increasingly difficult to distinguish extended sources from point sources as the off-axis angle increases. To overcome this, we used all 3334 of the $S/N > 8$ sources in our survey to study statistically how source size varies as a function of position on the PSPC. The method used has been described previously (Nichol *et al.* 1997), but we include an overview here for completeness. Figure 1 shows the distribution of source size (as defined by the lengths of the major and minor axes of the best fit ellipses) as a function of off-axis angle. After collecting these data into 10 pixel bins, we were able to determine how the mean and FWHM of the distribution varied with off-axis angle. (Beyond an off-axis angle of 90 pixels, the dispersion in source sizes became too large to define a reliable FWHM, hence the imposition of criterion ii). Under the assumption of a Gaussian distribution, the FWHM values were converted into sigma values and a three sigma curve was determined by fitting a 4th order polynomial to the $[\text{mean} + 3\sigma]$ values. A source was defined to be extended if it had a major and/or a minor axis more than 3σ from the mean.

In total, 374 sources were found to meet criteria (i) through (v). These are listed in Appendix E in right ascension order. Wavelet count rates (cr_W) are given for each source in units of $1 \times 10^{-2} \text{ counts s}^{-1}$ (column 4). We note that duplicate entries, *e.g.* RX J0056.5-2730 – which was detected in two pointings, wp700528 and rp701223n00 – have not been excised from this list. The fluxes for these 374 sources (assuming thermal spectra see §6.2) range from $0.2 \lesssim f_{-13} \lesssim 40$. In the interests of completing the optical follow-up in a timely fashion, it was decided to concentrate only on the brightest of these 374. An arbitrary count rate cut ($cr_W > 0.01163$) was imposed to reduce the sample size to roughly 100 (criterion vi). At the redshift of the most distant cluster in the EMSS sample ($z=0.81$), this count rate corresponds to a luminosity of $\simeq 3.9L_{44}$, which is approximately equal to locally determined values of L_* , *e.g.* $L_* = 5.7L_{44}$ (Ebeling *et al.* 1997), $L_* = 3.8L_{44}$ (De

Grandi *et al.* 1999a).

The total areal coverage of the Bright SHARC survey is 178.6 square degrees. This value was determined by calculating the area available for candidate detection in each of the 460 pointings in the survey. This area includes all pixels at radii greater than 2'.5 and less than 22'.4 which (i) had exposure times more than half that of the central pixel and (ii) did not overlap pixels in a higher exposure pointing. (There were 21 pairs of pointings with some overlap between them.)

5. IDENTIFICATION OF EXTENDED SOURCES

We present the 94 unique⁷ extended sources in the Bright SHARC survey in Table and Appendix C. For each candidate, we provide the source name (column 1), its J2000 position (columns 2 & 3), the wavelet count rate [0.4-2.0 keV] (cr_W in units of $1 \times 10^{-2} \text{ counts s}^{-1}$ column 4), the pointing in which it was detected (column 5), the source type (column 6), and the method used to identify the source (column 7). Alternate source names and redshifts (where available) are listed in column 8. We note that Abell clusters (Abell 1958; Abell, Corwin & Olowin 1989) are denoted by ‘A’. Likewise for EMSS sources (‘MS’, Stocke *et al.* 1991), 160 deg² clusters (‘V’, Vikhlinin *et al.* 1998a, V98 hereafter), Hickson groups (‘HCG’, Hickson 1982) and Zwicky clusters (‘Z’, Zwicky *et al.* 1968). When an object is listed in more than one catalog, we have defaulted to the name given in the older catalog, *e.g.* for RX J0237.9 we have listed the Abell number (A3038), not the V98 number (V28).

In Appendix C, we present small (6'.6 × 6'.6) Digitized Sky Survey (DSS) images of each of the 94 extended sources listed in Table. The source outlines, as defined by our friends-of-friends analysis are overlaid on these images. We note that the source centroids were defined in a weighted fashion and do not necessarily coincide with the geometric center of the source outline. No external astrometric solution was applied before making these DSS images, because the expected pointing offset is much smaller ($\lesssim 6''$) than the typical size of one of our extended sources.

In some cases it was possible to identify the source using the DSS images alone. For example, the X-ray emission from source RX J0324.6-5103 is clearly associated with a bright star (HD21360). This source was flagged as extended because emission from the star was blended by the friends-of-friends analysis with the (fainter) emission from a neighboring point source. (The X-ray surface brightness contours for this source show a secondary peak centered on the faint DSS object to the lower left of the source outline.) In other cases, the source outline, and/or the surface brightness contours, are indicative of blended emission but no obvious counterpart could be found on the DSS images, *e.g.* RX J0947.8+0741. When the DSS (or X-ray) images played a role in the identification of a source, a ‘D’ (or ‘X’) is listed in column 7 of Table.

A search of the NASA/IPAC Extragalactic Database (NED) has also provided useful information for several of the Bright SHARC extended sources, including some cluster redshifts *e.g.* for RX J1204.0+2807 (MS1201.5, Gioia *et al.* 1990). When NED yielded information was used during the source identification, an ‘N’ is listed in column 7

⁷Duplicate entries for RX J0237.9-5224 and RX J1211.2+3911 have been removed.

of Table .

Optical follow-up of Bright SHARC extended sources has been carried out at a number of telescopes; the 3.5m ARC telescope at Apache Point Observatory, the Danish 1.5-m and 3.6-m telescopes at the ESO Southern Observatories, the 1.5-m telescope at the Cerro Tololo Inter-American Observatory, the 3.6-m Canada France Hawaii Telescope on Mauna Kea and the 4-m Mayall telescope at Kitt Peak National Observatory. Optical follow-up includes CCD imaging, long slit spectroscopy and multi-object spectroscopy. Of the 94 extended sources, to date 57 have CCD images and 51 have been the target of spectroscopic follow-up. A ‘C’ in column 7 of Table indicates that a CCD image is available, whereas an ‘S’ indicates spectroscopic follow up by the SHARC collaboration and an ‘O’ indicates that spectroscopy came from private communications. To date, 91 of the 94 Bright SHARC extended sources have been identified; 37 clusters, 41 blends, 9 galaxies and 3 galaxy groups. The symbols ‘+’ in column 8 indicate that the identification of one of the components of a blended source is unknown. We note that the distinctions between galaxies and groups (see §7.4), and between groups and clusters, are not absolute at the low luminosity end. For the 12 extended objects (9 galaxies and 3 groups) at redshifts less than $z = 0.07$, we based our classifications on the information provided by NED.

6. THE BRIGHT SHARC CLUSTER SAMPLE

The thirty-seven clusters in the Bright SHARC are listed in Table 2. For each cluster, we list the source number (column 1), the cluster redshift (column 2), the hydrogen column density (in units of $1 \times 10^{20} \text{ cm}^{-2}$, column 3), the major and minor axes (in units of $14.''947$ pixels, columns 4 & 5), the offaxis angle of the cluster centroid (in units of $14.''947$ pixels, column 6), the wavelet (cr_W) and total (cr_T) count rates [0.4-2.0 keV] (in units of 1×10^{-2} counts s^{-1} , columns 7 & 8), the percentage error on cr_T (δcr_T , column 9), the aperture containing 80% of the flux from a model cluster profile (r_{80} , column 10, see §6.1), the fraction of that aperture used to measure the cluster count rate (f_{80} , column 11), the total flux [0.5-2.0 keV] (f_{-13} , in units of $1 \times 10^{-13} \text{ erg s}^{-1} \text{ cm}^{-2}$, column 12), the corresponding luminosity (L_{44} , in units of $1 \times 10^{44} \text{ erg s}^{-1}$, column 13), and the temperature used to derive the flux and luminosity (T, in units of keV, column [14]). Various notes, including alternative cluster names and pointers to the information on the pointing target (if that target was a cluster) are given in column (15).

The redshift distribution ($\bar{z}=0.266$) for the 37 Bright SHARC clusters is shown in Figure 3. The highest redshift, and most luminous, cluster in the sample is RX J0152.7 ($z=0.83$). The lowest redshift cluster in the sample is RX J0321.9 ($z=0.0696$). Twenty-one of the redshifts in Table 2 are presented here for the first time. These 21 include 17 clusters which have not been listed before in any published catalog and 4 clusters from the 160 deg^2 survey (V98). We describe below how the count rates (§6.1) and fluxes/luminosities (§6.2) were derived.

6.1. Total Cluster Count rate Derivation

The method described in §4, to measure wavelet count rates for all 10,277 sources in the Bright SHARC survey, was adopted because it was easy to apply to large num-

bers of sources. However, the method is not optimal for measuring cluster fluxes. This is because no correction is made for cluster flux falling outside the zero crossing boundary. Moreover, when a portion of a cluster overlaps a masked out region (*e.g.* regions in the shadow of the support struts), the flux from that region will not be included in the count rate. Therefore, for the 37 sources identified with clusters of galaxies, we have performed a second count rate determination based on the method adopted by Holden *et al.* (1997). For each of the clusters, we derived an aperture for the flux measurement using a cluster model based on a modified isothermal sphere:

$$I = \frac{I_0}{[1 + (r/r_c)^2]^{3\beta-1/2}}, \quad (2)$$

where I is the surface brightness at radius r . We used values for the slope ($\beta = 0.67$) and core radius ($r_c = 250 \text{ kpc}$) which are typical for rich clusters (Jones & Forman 1992) and then converted the model from physical units to angular units using the cluster redshift. The cluster models were convolved with the appropriate off-axis PSPC PSF (Nichol *et al.* 1994a) so that the radius of a circular aperture, r_{80} , which contained $\simeq 80\%$ of the total model flux could be defined (for $\beta = \frac{2}{3}$, $r_{80} = \sqrt{24}r_c$). The choice of r_{80} for the aperture represents a compromise between including a high fraction of the cluster flux and keeping down the number of contaminating sources within the region.

The 80% radii, r_{80} , are listed in column 10 of Table 2, in units of $14.''947$ pixels. Since these radii could be quite large, up to 40 pixels, some of them overlapped other sources. If any $r < r_{80}$ pixels lay within the wavelet-defined boundary of another source, they were masked out from the cluster aperture. Also masked were any pixels that received less than half the exposure time of the central pixel in the count rate map. By reference to the cluster model, it was possible to correct for the fraction of cluster flux lying in these masked regions. In column 11 of Table 2, we list the fraction of the 80% aperture available for flux determination, f_{80} . The raw aperture count rates for each of the 37 clusters were measured by summing the flux in the unmasked $r < r_{80}$ pixels.

The corresponding background count rates were measured inside 120×120 pixel boxes centered on the cluster position. The background levels were measured in annuli with minimum radii of $1 \times r_{80}$ and maximum radii $3 \times r_{80}$. If these annuli overlapped any source boundaries, any low exposure pixels, or the edges of the 120×120 pixel box, the pixels in those regions were excluded from the background calculations. In Appendix D we illustrate the masked out regions for the source and background apertures for each of the 37 Bright SHARC clusters. After subtraction of the appropriately scaled background, the total cluster count rates were derived by dividing by $(0.8 \times f_{80})$. The background subtracted, aperture corrected, total cluster count rates (cr_T) are listed in column 8 of Table 2. The one sigma errors on the total cluster count rates are listed in column 9 of Table 2. These errors were calculated by adding in quadrature the counting errors on the cluster count rates and the background count rates. We draw attention to three SHARC clusters with anomalously high ($> 15\%$) count rates errors; RX J0250.0, RX J1524.6, RX

J1222.1. These clusters have much lower signal to noise values inside the cr_T apertures than in the cr_W apertures, demonstrating that the adopted cluster model (equation 2) significantly over estimates the size of the aperture which encircles 80% of the source flux. The count rate errors are quoted as percentages since, in the absence of systematic errors in the count rate to flux/luminosity conversions (§6.2), they should also reflect the percentage errors on the flux (f_{-13} , column 12) and luminosity (L_{44} , column 13). In Figure 2 we compare the initial wavelet count rates, cr_W (column 7), to the total aperture corrected count rates, cr_T . It can be seen that, as expected, the total count rate is systematically higher than the wavelet count rate. A least squares fit to the clusters at redshifts greater than $z=0.15$ shows that the total count rate is typically 2.1 times higher than the wavelet value. At lower redshifts, the correction is higher because the clusters are significantly more extended than the $\sigma = 3$ pixel wavelet we used for source detection. It is encouraging that the wavelet count rate appears to be an unbiased measure of the total cluster count rate, since we have used the cr_W values to define the count rate limit of the Bright SHARC Survey.

6.2. Luminosity Derivation

We used the cr_T count rates listed in column 8 of Table 2 to determine fluxes and luminosities for each cluster. We note that we chose to present the fluxes and luminosities in the [0.5-2.0 keV] band, rather than in the Bright SHARC count rate band [0.4-2.0 keV], to allow easier comparison with other studies. Since the ROSAT PSPC provides only limited spectral resolution, we had to assume a spectral model for each cluster to make the conversion between measured cluster count rate and unabsorbed flux. As is typical in X-ray cluster analyses, we adopted an emission spectrum from hot, diffuse gas based on the model calculations of Raymond and Smith (Raymond & Smith 1977). The integrated emission from a Raymond-Smith spectrum in the SHARC energy band (observer's rest frame) depends on several factors; the metallicity and temperature of the gas, the redshift of the cluster, and the absorption column along the line of sight. This means that the conversion between measured aperture count rate and cluster luminosity is non trivial and must take into account the specific properties of each cluster. We note that, in most cases, the dominant source of error in the derived luminosities comes from the count rate uncertainty, which rises to 30% in the case of RX J1524.6. However, for those clusters with well determined count rates (30 clusters have count rate errors of less than 10%) it is worth making the extra effort to reduce the systematic errors in the conversion between count rates, fluxes and luminosities.

We have constructed a matrix of count rate to flux conversion factors as a function of temperature, redshift and absorbing column. (A single, canonical, value for the metallicity – one third the Solar value – was used throughout.) The conversion factors were derived using the `fakeit` command in XSPEC (version 10.00, Arnaud *et al.* 1996) together with the appropriate ROSAT PSPC response function. Photo-electric absorption was included via the XSPEC `wabs` model, which is based on cross sections presented in Morrison & McCammon (1983). The neutral

Hydrogen column densities adopted for each cluster are listed in column 3 of Table 2. These values were derived using the AT&T Bell Laboratories 21 cm survey (Stark *et al.* 1992), for clusters north of -40° , and the values presented in Dickey & Lockman (1990) for clusters at lower declinations. In order to sample the observed distribution of cluster redshifts and column densities, and the expected distribution of cluster temperatures, we derived conversion factors over the following ranges; (i) $0.06 < z < 0.86$ (in increments of $\delta z = 0.05$), (ii) $0 < nH < 20 \times 10^{20} \text{ cm}^{-2}$ (in increments of $1 \times 10^{20} \text{ cm}^{-2}$), and (iii) $1 < T < 12 \text{ keV}$ (in increments of 1 keV). (When a cluster redshift or column density was not exactly matched by one of the matrix entries, linear interpolation was used.) As expected, the count rate to flux conversion varied most rapidly along the column density axis of this matrix, however changing the redshift also had a measurable effect (by a factor of $\simeq 2$ over the range $0.08 < z < 0.8$). Estimates of the bolometric⁸ and k-corrections were also derived, as a function of temperature, using XSPEC.

The luminosity derivation included an iteration to obtain an estimate of the X-ray temperature for each cluster, using the luminosity-temperature (L-T) relation presented in Arnaud & Evrard (1999). From a starting point of $T=6 \text{ keV}$ an initial [0.5-2.0 keV] luminosity was derived. This luminosity was then converted into a pseudo bolometric luminosity, so that a temperature estimate (to the nearest integer in keV) could be derived. The new temperature was used to select a second count rate to flux conversion from the matrix and the process was repeated until convergence was reached. The temperature used in the final luminosity calculation is listed in column 14 of Table 2.

In the past, the luminosity-temperature (L-T) relation was not so well known and other groups have adopted a single temperature, usually 6 keV, for their luminosity calculations. Using the Arnaud & Evrard (1999) L-T relation, 6 keV corresponds to a cluster of $L_{44} \simeq 6$. Most of the clusters in Table 2 are significantly fainter than this, meaning that the use of a canonical temperature will yield inaccurate results, especially for the lowest luminosity clusters. This is illustrated by the faintest (and hence, coolest) cluster in our sample (RX J1524.6) which has a luminosity of $L_{44}=0.065$ when a temperature of $T=1 \text{ keV}$ is assumed and a luminosity of $L_{44}=0.072$ when a temperature of $T=6 \text{ keV}$ is assumed (an 11% effect). By contrast the effect is smaller (5%) for the hottest cluster in our sample; RX J0152.7 has a luminosity of $L_{44} = 8.26$ when a temperature of $T=9 \text{ keV}$ is assumed and a luminosity of $L_{44}=8.65$ when a temperature of $T=6 \text{ keV}$ is assumed. It is worth mentioning that the L-T relation we use (Arnaud & Evrard 1999) was constructed from clusters known not to contain cooling flows. Another recent work (Allen & Fabian 1998) combines both non-cooling flow and cooling flow clusters and fits a flatter slope to the L-T relation (2.4 compared to 2.9). Unfortunately, the poor photon statistics of the Bright SHARC cluster sample do not allow us to test for the presence of cooling flows and so our choice of L-T relation will be inappropriate in some cases.

Finally, we note that the conversion between cluster count rate and cluster luminosity is a function of the adopted

⁸An energy range of 0.01-50 keV was used to calculate the (pseudo) bolometric corrections, which were found to be in excellent agreement with those presented in Figure 2 of Borgani *et al.* 1999.

values of Hubble’s Constant and the deceleration parameter and that we have used $H_0=50 \text{ km s}^{-1} \text{ Mpc}^{-1}$ and $q_0=0.5$ throughout.

7. DISCUSSION

In a companion paper (Nichol *et al.* 1999, N99 hereafter) we use the Bright SHARC sample to examine evolution in the X-ray cluster luminosity function (XCLF). Future papers will go on to use these evolution results to constrain the density parameter Ω_m . It is appropriate, therefore, to discuss here some of the observational issues relevant to Ω_m analyses. These issues include systematic biases in the derived luminosities (§7.1) of the Bright SHARC clusters and any possible contamination (§7.2), or incompleteness (§7.3) in the Bright SHARC catalog. We also discuss the possible discovery of three “fossil groups” (§7.4) and our overlap with the 160 deg² survey of V98 (§7.5).

7.1. Luminosity Bias in the Bright SHARC Cluster Sample

A systematic bias in our luminosities would result in an over (or under) estimate of the number density of high luminosity systems. To investigate whether such a systematic bias exists, we have compared the luminosities quoted in column 13 of Table 2 with published values for the six clusters we have in common with the EMSS (Gioia *et al.* 1990): RX J1024.3 (MS1020.7 or A981), RX J1204.0 (MS1201.5), RX J1211.2 (MS1208.7), RX J1222.1 (MS 1219.9), RX J1311.2 (MS1308.8), RX J2258.1 (MS2255.7 or Z2255.5). We have chosen to compare our luminosities for these clusters with those presented in Nichol *et al.* (1997, N97 hereafter), rather than those presented in Henry *et al.* (1992), for two reasons. First the luminosities quoted in N97 are in the ROSAT bandpass [0.5-2.0 keV] rather than the Einstein bandpass [0.3-3.5 keV]. Second, the N97 study used the SHARC pipeline to produce count rate maps. A comparison of the two sets of luminosities will, therefore, show if the methodology outlined in sections §6.1 and §6.2 is robust (since a different methodology⁹ was used in N97). We find our derived luminosities to differ by 0% for MS1020.7, 1% for MS1201.5, 5% for MS1208.7, 26% for MS1219.9, 2% for MS1303.8 and 10% for MS1219.9. These differences are all smaller than the 1 sigma errors on the EMSS count rates quoted in N97. We note also that the luminosity we derive for RX J0152.7 is within 1% of the value derived by the WARPS collaboration in Ebeling *et al.* (1999).

We have also compared the fluxes quoted in column 12 of Table 2 with published values for the 11 clusters we have in common with the 160 deg² survey (V98, see §7.3). In Table 3, column 5, we present the ratio of Bright SHARC to V98 fluxes. We find the Bright SHARC values to be systematically higher than those measured by V98, with an average flux ratio of 1.18. To understand this discrepancy, we have recalculated the Bright SHARC fluxes using the core radii and redshifts presented in V98. Except for RX J1641.2, the V98 core radii are all smaller than $r_c=250\text{kpc}$ and, by using their values, we bring the average flux ratio down to 1.01 (column 6).

We conclude that the methodology of sections §6.1 & §6.2 is robust, although it has the disadvantage of over esti-

imating the cluster flux if $r_c < 250\text{kpc}$. Planned XMM observations of several Bright SHARC clusters will provide higher angular resolution and signal-to-noise images together with accurate estimates of the electron temperature. These observations will provide an important test of the methods described in sections §6.1 & §6.2 since they will allow us to (i) more accurately excise contaminating sources in the cluster aperture, (ii) use fitted, rather than canonical, values for β , r_c and the ellipticity, (iii) be less sensitive to errors in the background calculation and (iv) improve our spectral dependent count rate to flux conversions.

7.2. Contamination of the Bright SHARC Cluster Sample

The thorough, multi-object, spectroscopic follow-up of the Bright SHARC extended source list means that it is highly unlikely that any of the entries in Table 2 are mis-identified contaminants. However, we stress that there are two clusters in that table which should *not* be used for studies of the cluster XCLF because their detections are not truly serendipitous: RX J1024.3 and RX J1541.1 were found in cluster pointings and lie at redshift separations from the pointing target of $\delta z < 0.002$, or $cz < 600 \text{ km s}^{-1}$. These clusters are probably associated with the pointing target via the cluster correlation function (Romer *et al.* 1994; Nichol *et al.* 1994b). In addition, we feel that RX J1222.1 (MS1219.9) warrants further study: This object is very compact, has a large count rate uncertainty (§6.1) and Gioia & Luppino (1994) note that its central galaxy has emission lines. It is possible, therefore, that the luminosity quoted in Table 2 is an overestimate due to AGN contamination. (Although, it should be noted that the presence of emission lines in the central galaxy could be attributed to cooling flow nebulosity or star formation, Crawford *et al.* 1999.) We note that the three clusters highlighted here (RX J1024.3, RX J1222.1 & RX J1541.1) have redshifts in the range $0.20 < z < 0.25$ and so were not used in the N99 analysis (which concentrated only on those clusters at $z > 0.3$).

7.3. Incompleteness of the Bright SHARC Cluster Sample

There are three possible ways in which the Bright SHARC cluster sample might be incomplete. First there are those clusters that did not meet our selection criteria. Second, there is a possibility that some clusters were misidentified as contaminants. Third, there are the three extended sources which have yet to be identified.

We are using simulations to understand how the adopted selection criteria (§4) effects the completeness of the Bright SHARC cluster sample. We are in the process of carrying out a very thorough investigation of our selection function by adding many thousands of fake clusters (one at a time) to the pointings in our survey and then determining the fraction of these fake clusters that would have been selected as Bright SHARC cluster candidates. These simulations will provide us with the efficiency of cluster detection as a function of cluster parameters (*e.g.* redshift, luminos-

⁹Differences between Bright SHARC and N97 include the use of the IRAF PROS package to set background apertures and the use of a constant temperature, $T=6 \text{ keV}$, for k-corrections and count rate to flux conversions.

ity, ellipticity, core radius *etc.*) and operational parameters (*e.g.* exposure time, off-axis angle, Hydrogen column density, central target *etc.*). The results of these simulations will be presented elsewhere (Adami *et al.* 1999), but our preliminary findings are described in N99.

Let us now address possible cases where clusters might be misidentified as contaminants. We discuss first the two objects listed in Table as blends of a cluster with another source, RX J0318.2 & RX J2314.7. The former, RX J0318.2, is a blend of a cluster with a QSO. (The cluster has the same redshift as the neighboring cluster RX J0318.8, $z=0.37$). The surface brightness contours of RX J0318.2 are clearly dumb-bell shaped and so it has been possible to remove the QSO contribution from the total count rate. This object was also discovered as part of the Southern SHARC and Burke (1998) has determined the total count rate and luminosity of this cluster to be $cr_T=0.01362$ count s^{-1} and $L_{44} = 1.11$ respectively. Therefore, this cluster would not have made it into the Bright SHARC sample had it not been blended with the QSO and its exclusion for Table 2 is justified. By contrast, the boundary between the cluster and M-star emission for RX J2314.7 is blurred. Hence it is not possible to excise the M-star flux to see if the cluster alone has a high enough count rate (and extent) to qualify as a Bright SHARC candidate. If the M-star makes only a minimal contribution, less than 20%, to the total flux, then the cluster should have been included in Table 2: Assuming that all the RX J2314.7 flux comes from the cluster, the cluster would have a luminosity of $L_{44}=1.31$.

As stated above, three of the 94 Bright SHARC extended sources remain unidentified. If all three were high redshift, high luminosity clusters, then there would be important implications for cluster evolution. In N99, we predict that the Bright SHARC survey should include 4.9 clusters with luminosities $L_{44} \geq 5$ in the redshift range $0.3 < z < 0.7$ (based on a simple extrapolation of the De Grandi *et al.* 1999b local XCLF). Since only 1 such cluster has been confirmed to exist in the Bright SHARC (RX J1120.1), we conclude in N99 that there may be evidence for evolution at luminosities brighter than $L_{44} = 5$. This evidence would effectively disappear if another 3 Bright SHARC clusters were added in this luminosity range. We stress, however, that it is very unlikely all these objects are clusters with luminosities brighter than $L_{44} = 5$; the CCD images of RX J0340.1 & RX J1705.6 are not consistent with the presence of distant clusters and RX J1838.8 is in a crowded star field (and so is most likely associated with a stellar X-ray source). We conservatively estimate that one of these objects may be a cluster, given that the ratio of clusters to non-clusters among the other 91 identified sources is roughly 1:3. We have calculated that this cluster would have to reside at $z > 0.62$, $z > 0.57$ or $z > 0.51$, for RX J0340.1, RX J1705.6 and RX J1838.8 respectively, to have a luminosity greater than $L_{44} = 5$.

We also highlight candidate RX J1210.4. This object contains a QSO and has a compact X-ray surface brightness profile. Even though most of the flux from this source is probably coming from the QSO, this object merits further study since a CCD image highlights a clustering of faint galaxies around the bright central object. The redshift of this

source ($z=0.615$) and its high count rate ($cr_W = 0.1430$) mean that if more than 18% of the count rate from this source was coming from an associated cluster, then this cluster would have a luminosity greater than $L_{44}=5$.

For the various reasons outlined above, we have decided to continue the follow-up of the Bright SHARC in a variety of ways. As a first priority, we plan to identify the three remaining unidentified Bright SHARC extended sources (RX J0340.1, RX J1705.6 and RX J1838.8). We also plan to obtain identifications for at least one portion of the seven “id-pending” blends listed in Table and to continue our campaign to obtain velocity dispersions for the Bright SHARC clusters. Moreover, we hope to obtain higher resolution X-ray images of complex sources such as RX J1210.4, RX J1222.1 and RX J2314.7, to help determine the contamination level.

7.4. Fossil Groups and Dark Clusters in the Bright SHARC Survey

We present evidence for the discovery of three new “fossil groups” (Ponman *et al.* 1994) or X-ray Over-Luminous Elliptical Galaxies (OLEGs, Vikhlinin *et al.* 1999). These objects are predicted to occur when a galaxy group relaxes to form a single elliptical galaxy. They are interesting because they provide invaluable insight into the processes of elliptical galaxy evolution, metal enrichment in the intra cluster medium, and the dynamics of extended dark halos (Mulchaey & Zabludoff 1998). Their observational signatures would be an isolated cD or giant elliptical galaxy surrounded by a cool ($T \approx 1$ keV), extended, X-ray halo. Two galaxies detected in the Bright SHARC survey appear to share these properties; RX J1730.6 (NGC6414, $z=0.05$) and RX J0327.9 (UGC2748, $z=0.03$). Applying the same method used to obtain total cluster count rates (§6.1), we have measured their luminosities to be $L_{44}=0.158$ and $L_{44}=0.056$ respectively¹⁰. In addition to these two galaxies, one of the Bright SHARC clusters, RX J0321.9 (A3120, $z=0.0696$, $L_{44} = 0.43$), also appears to display “fossil group” characteristics. We highlight these objects here since they are ideal targets for follow-up studies at X-ray and optical wavelengths. We have estimated the “fossil group” space density to be $\sim 2 \times 10^{-6} \text{Mpc}^{-3}$ under the assumption that the Bright SHARC is 100% efficient in detecting extended sources in the redshift range $0.02 < z < 0.08$ and at luminosities of $L_{44} > 0.1$.

In addition to estimating the space density of “fossil groups”, we can comment on the space density of “dark clusters” or “failed clusters”. These objects are theorized to have cluster-like masses, and to radiate in the X-rays, but to have an under luminous galactic component (Tucker *et al.* 1995; Hattori *et al.* 1997). We have successfully identified 91 of the 94 Bright SHARC extended sources and have found no evidence for “dark clusters”. To avoid detection in the Bright SHARC, these objects either must have a lower space density than rich clusters and “fossil groups”, or they must be intrinsically faint and evolve rapidly (to avoid detection at low redshift). In either case, “dark clusters” are unlikely to be a significant contribution to the mass of the universe.

7.5. Comparison with the 160 deg² Survey

¹⁰Assuming an absorbed Raymond Smith spectrum with an electron temperature of $T=1$ keV.

As pointed out by N99, it may be possible to combine the Bright SHARC with the 160 deg² survey (V98), to maximize the area available for high redshift cluster searches. The motivation for this is demonstrated by Figure 3, which shows several gaps in the redshift coverage of our survey. Even though we are able to find high luminosity clusters out to at least $z = 0.83$, we find none at $z \simeq 0.5$ or $z \simeq 0.7$. The only way to guarantee more $L_{44} > 3$ cluster detections would be to search over a wider area. The combination of the two surveys would yield a search area of $\simeq 260$ deg², since only 44% (or $\simeq 78$ deg²) of the Bright SHARC Survey overlaps with the 160 deg² survey. (There are 201 pointings in common between the 160 deg² and Bright SHARC Surveys; Alexey Vikhlinin, private communication).

There are 13 sources in common between the Bright SHARC and the 160 deg² surveys. Of these 13, five clusters have not been followed up spectroscopically by either survey but rely on literature redshifts (RX J1010.2¹¹, RX J1204.0, RX J1211.2, RX J1311.2, RX J2258.1). An additional three clusters have both Bright SHARC and V98 redshifts (RX J0849.1, RX J1406.9, RX J1701.3); with the two redshifts being in agreement in all cases. We have also been able to provide spectroscopic information for five 160 deg² sources which previously relied on photometric redshifts; RX J0237.9 (V28), RX J0947.8 (V75), RX J1418.5 (V159), RX J1524.6 (V170), RX J1641.2 (V183). We have identified RX J0947.8 as a blend, the main component of which is a QSO¹² at $z=0.63$ (Burke 1998). We confirm that the other four sources are clusters and we find that the photometric redshifts listed in V98 are good estimates of the true redshift, with the largest error being $\delta z = 0.065$ for RX J1641.2. This cluster has been shown to be at $z = 0.195$, giving it a luminosity of $L_{44} = 1.355$. It is not, therefore, a high redshift, high luminosity, cluster, as previously suggested by Vikhlinin *et al.* (1998b), based on the upper limit of the estimated redshift ($z_{est} = 0.26_{-0.07}^{+0.04}$). In addition to the 13 sources described above, 77 other V98 clusters were detected in the 201 pointings common to the two surveys. Most of these clusters are too faint to have been included in the Bright SHARC sample, only 9 have wavelet count rates greater than the Bright SHARC threshold ($cr_W = 0.01163$). Of these 9, seven were not included in the Bright SHARC because they did not meet our filling factor criterion ($f < 1.3$), one was detected at an offaxis distance less than our threshold of 2'.5 and one did not meet our extent criterion. Conversely, two clusters (RX J0256.5 and RX J1311.8) in Table 2 are not listed in V98, despite falling in common pointings, because they lie beyond the V98 offaxis limit of 17'.5. These examples demonstrate how differing survey selection criteria produce differing cluster samples and that detailed simulations are required to determine a survey's selection

function.

There are eight confirmed $L_{44} > 3$ clusters in the Bright SHARC; RX J0152.7, RX J0256.5, RX J0318.5, RX J0426.1, RX J1241.5, RX J1120.1, RX J1334.3, RX J1701.3. The presence of so many $L_{44} > 3$ clusters in the Bright SHARC has allowed us to show that the XCLF is non-evolving up to $L_{44} \simeq 5$ (N99). It is important to note that, even after the combination of Bright SHARC and 160 deg² surveys, the areal coverage available for high redshift cluster searches will still be only about one third that of the EMSS at the bright end (Henry *et al.* 1992). This means that we will probably have to wait until larger area surveys are made available, e.g., from the XMM satellite (Romer *et al.* 2000), to make definitive statements about XCLF evolution at $L_{44} > 5$.

Appendices A through E have been omitted from the astro-ph submission.¹³

Acknowledgements

We acknowledge financial support from NASA grants NAG5-2432 (AR, RP, CA & MU), NAG5-6548 (RN), NAG5-3202 (BH), GO-06838.01-95A (BH). And also from a NASA Space Consortium Grant through Aerospace Illinois (AM, KC, BH), the CMU undergraduate research initiative (AJM), the NSF Center for Astrophysical Research in Antarctica (BH), NSF grant AST-9256606 (BH) and PPARC (DB). This research has made use of: (i) Data obtained through the High Energy Astrophysics Science Archive Research Center Online Service, provided by the NASA-Goddard Space Flight Center. (ii) The Digitized Sky Survey which was produced at the Space Telescope Science Institute under US Government grant NAG W-2166. (iii) The NASA/IPAC Extragalactic Database (NED) which is operated by the Jet Propulsion Laboratory, Caltech, under contract with the National Aeronautics and Space Administration. (iv) The "APM Catalogues at AAO" web server, author Micheal Drinkwater. (v) The APS Catalog of POSS I and the APS Image Database, which are supported by the National Science Foundation, the National Aeronautics and Space Administration, and the University of Minnesota. We offer special thanks to Jim DeVeney and the support staff at the ARC, CFHT, CTIO, ESO & KPNO telescopes, and also to Alain Blanchard, Francisco Castander, Ian Del Antonio, Paul Lynam, Eric Monier, Francis Falbo, Tim Kimball, Marc Postman, Patricia Purdue, Connie Rockosi, Rachid Sadat, Steve Snowden, Jeffrey Tran, Dave Turnshek, Pedro Viana, Alexey Vikhlinin and an anonymous referee.

REFERENCES

- Abell, G. O. 1958, ApJS, 3, 211.
 Abell, G. O., Corwin, H. G. & Olowin, R.P. 1989, ApJS, 70, 1.
 Adami, C. Ulmer, M.P., Holden, B.P., Romer, A.K., Nichol, R.C., Pildis, R.A. 2000, ApJS, in press.
 Bahcall, N.A., Fan, X. 1998, ApJ, 504, 1.
 Allen, S.W., Edge, A.C., Fabian, A.C., Böhringer, H., Crawford, C.S, Ebeling, H., Johnstone, R.M., Naylor, T., Schwarz, R.A. 1992, MNRAS, 259, 67.
 Allen, S.W., Fabian, A.C. 1998, MNRAS, 297, 57.
 Arnaud, K.A. 1996, ASP Conf. Series, 101, 17.

¹¹RX J1010.2 was not included in Table 2 because its redshift ($z=0.045$) is too low, *i.e.* $z < 0.07$.

¹²Subsequent observations by Vikhlinin *et al.* have shown that this QSO most likely resides on the outskirts of a cluster at the same redshift (Alexey Vikhlinin, private communication).

¹³The appendices are accessible from <http://www.journals.uchicago.edu/ApJ/journal/issues/ApJS/v126n2/40418/40418.html>

- Arnaud, M. & Evrard, A.E. 1999, MNRAS, 305, 631.
- Böhringer, H., Guzzo, L., Collins, C.A., Neumann, D.M., Schindler, S., Schuecker, P., Cruddace, R., Chincarini, G., De Grandi, S., Edge, A.C., Macgillivray, H.T., Shaver, P., Vettolani, & G., Voges, W. 1998, in *Wide Field Surveys in Cosmology*, ed. S. Colombi, Y. Mellier, B. Raban (Gif-sur-Yvette; Editions Frontiers), 261.
- Borgani, S., Rosati, P., Tozzi, P., & Norman, C. 1999, ApJ, 515, 40.
- Boyle, B.J., McMahon, R.G., Wilkes, B.J., Elvis, M. 1995, MNRAS, 272, 462.
- Burke, D.J., Collins, C.A., Romer, A.K., Holden, B.P., & Nichol, R.C. 1997, ApJ, 488, L83.
- Burke, D. 1998, PhD Thesis, University of Durham.
- Carballo, R., Warwick, R.S., Barcons, X., Gonzalez-Serrano, J.I., Barber, C.R., Martinez-Gonzalez, E., Perez-Fournon, I., & Burgos, J. 1995, MNRAS, 277, 1312.
- Carlberg, R.G., Morris, S.L., Yee, H.K.C., & Ellingson, E. 1997, ApJ, 479, L19.
- Castander, F.J., Bower, R.G., Ellis, R.S., Aragon-Salamanca, A., Mason, K.O., Hasinger, G., McMahon, R.G., Carrera, F.J., Mittaz, J.P.D., Perez-Fournon, I., & Lehto, H.J. 1995, Nature, 281, 59.
- Collins, C.A., Burke, D.J., Romer, A.K., Sharples, R.M., & Nichol, R.C. 1997, ApJ, 479, L117.
- Couch, W.J., Ellis, R.S., Malin, D.F., MacLaren, I. 1991, MNRAS, 249, 606.
- Crawford, C.S., Allen, S.W., Ebeling, H., Edge, A.C. & Fabian A.C. 1999, MNRAS, 306, 857.
- Dalton, G.B., Efstathiou, G., Maddox, S.J., & Sutherland, W.J. 1994, MNRAS, 269, 151.
- De Grandi, S., Guzzo, L., Böhringer, H., Molendi, S., Chincarini, G., Collins, C., Cruddace, R., Neumann, D., Schindler, S., Schuecker, P. & Voges, W. 1999a, ApJ, 513, L17.
- De Grandi, S., Böhringer, H., Guzzo, L., Molendi, S., Chincarini, G., Collins, C., Cruddace, R., Neumann, D., Schindler, S., Schuecker, P. & Voges, W. 1999b, ApJ, 514, 148.
- De Vaucouleurs, G., De Vaucouleurs, A., Corwin Jr., H.G., Buta, R.J., Paturel, G. & Fouque, P. 1991, *Third Reference Catalogue of Bright Galaxies*, Volume 1-3, XII, Springer-Verlag.
- Dickey, J.M., & Lockman, F.J. 1990, ARAA, 28, 215.
- Ebeling, H., Voges, W., Böhringer, H., Edge, A.C., Huchra, J.P., & Briel, U.G. 1996, MNRAS, 281, 799.
- Ebeling, H., Edge, A.C., Fabian, A.C., Allen, S.W., Crawford, C.S., Böhringer, H. 1997, ApJ, 479, L101.
- Ebeling, H., Edge, A.C., Böhringer, H., Allen, S.W., Crawford, C.S., Fabian, A.C., Voges, W., & Huchra, J.P. 1998, MNRAS, 301, 881.
- Ebeling, H., Jones, L.R., Perlman, E., Sharf, C., Horner, D., Wegner, G., Malkan, M., Fairley, B., Mullis, C.R. 1999, ApJ, submitted, astro-ph/9905321.
- Fairall, A.P., Willmer, C.N.A., Calderon, J.H., Latham, D.W., Nicolaci da Costa, L., Pilligrini, P.S., Nunes, M.A., Focardi, P., & Vettolani, G. 1992, AJ, 103, 11.
- Gioia, I. M., Henry, J.P., Maccacaro, T., Morris, S.L., Stocke, J.T., Wolter, A. 1990, ApJ, 356, L35.
- Gioia, I.M. & Luppino, G.A. 1994, ApJS, 94, 583.
- Gioia, I.M., Henry, J.P., Mullis, C.R., Ebeling, H., Wolter, A., 1999, AJ, 117, 2608.
- Hasinger, G., Turner, T.J., George, I.M., & Boese, G. 1992, Legacy 2, 77.
- Hattori, M., Ikebe, Y., Asaoka, I., Takeshima, T., Böhringer, H., Mihara, T., Neumann, D.M., Schindler, S., Tsuru, T., & Tamura, T. 1997, Nature, 388, 146.
- Henry, J.P. 1997, ApJ, 489, L1.
- Henry, J.P., Gioia, I.M., Maccacaro, T., Morris, S.L., Stocke, J.T., & Wolter, A. 1992, ApJ, 386, 408.
- Henry, J.P., Gioia, I.M., Mullis, C.R., Clowe, D.I., Luppino, G.A., Böhringer, H., Briel, U.G., Voges, W., & Huchra, J.P. 1997, AJ, 114, 1293.
- Hewitt, A., & Burbidge, G. 1993, ApJS, 87, 451.
- Hickson, P., De Oliveira, C.M., Huchra, J.P., & Palumbo, G.G.G. 1992, ApJ, 339, 353.
- Hickson, P. 1982, ApJ, 255, 382.
- Holden, B.P., Romer, A.K., Nichol, R.C., & Ulmer, M.P. 1997, AJ, 115, 1701.
- Huchra, J.P., Henry, J.P., Postman, M., Geller, M.J. 1990, ApJ, 365, 66.
- Jones, C. & Forman, W. 1992, in *Clusters and Superclusters of Galaxies*, edited by A.C. Fabian (Kluwer, Dordrecht), 49. not find one?
- Jones, L.R., Scharf, C., Ebeling, H., Perlman, E., Wegner, G., Malkan, M., & Horner, D. 1998, ApJ, 495, 100.
- Lobo, C., Lazzati, D., Iovino, A., Guzzo, K., & Chincarini, G., in *Wide Field Surveys in Cosmology*, ed. S. Colombi, Y. Mellier, B. Raban (Gif-sur-Yvette; Editions Frontiers), 239.
- Longhetti, M., Rampazzo, R., Bressan, A., & Chiosi, C. 1998, A&AS, 130, 367.
- Lumsden, S. L., Nichol, R.C, Collins, C. A., & Guzzo, L. 1992, MNRAS, 258, 1.
- Morrison, R., & McCammon, D. 1983, ApJ, 270, 119.
- Mulchaey, J.S. & Zabludoff, A.I. 1998, ApJ, 514, 133.
- Nichol, R.C., Ulmer, M.P., Kron, R.G., Wirth, G., & Koo, D.C. 1994a, ApJ, 432, 464.
- Nichol, R.C., Briel, O.G., Henry, J.P. 1994b, MNRAS, 267, 771.
- Nichol, R.C., Holden, B.P., Romer, A.K., Ulmer, M.P., Burke, D.J., & Collins, C.A. 1997, ApJ, 481, 644.
- Nichol, R.C., Romer, A.K., Holden, B.P., Ulmer, M.P., Pildis, R.A., Adami, C., Merrelli, A.J., Burke, D.J. & Collins, C.A. 1999, ApJ, 521, L21.
- Oukbir, J. & Blanchard, A. 1992, A&A, 262, L21.
- Perlman, E.S., Padovani, P., Giommi, P., Sambruna, R., Jones, L.R., Tzioumis, A., & Reynolds, J. 1998, AJ, 115, 1253.
- Postman, M., Lubin, L. M., Gunn, J. E., Oke, J. B., Hoessel, J. M., Schneider, D. P., & Christensen, J. A. 1996, AJ, 111, 615.
- Ponman, T.J., Allan, D.J., Jones, L.R., Merrifield, M., McHardy, I.M., Lehto, H.J., & Luppino, G.A. 1994, Nature, 369, 462.
- Raymond, J.C., & Smith, B.W. 1977, ApJS, 35, 419.
- Reichert, D.E., Nichol, R.C., Castander, F.J., Burke, D.J., Romer, A.K., Holden, B.P., Collins, C.A., & Ulmer, M.P. 1999, ApJ, 518, 521.
- Reimers, D., Toussaint, F., Hagen, H.-J., Hippelein, H., & Meisenheimer, K. 1997, A&A, 326, 489.
- Romer, A.K., Collins, C.A., Böhringer, H., Cruddace, R.G., Ebeling, H., Macgillivray, H.G., Voges, W. 1994, Nature, 372, 75.
- Romer, A.K. 1995, PhD Thesis, University of Edinburgh.
- Romer, A.K., Viana, P.T.P., Liddle, A.R., & Mann, R.G., 2000, ApJ, submitted (astro-ph/9911499).
- Rosati, P., Della Ceca, R., Norman, C., & Giacconi, R. 1998, ApJ, 492, 21.
- Sadat, R., Blanchard, A., & Oukbir, J. 1998, A&A, 329, 21.
- Slezak, E., Bijaoui, Mars, G. 1990, A&A, 227, 301.
- Slinglend, K., Batuski, D., Miller, C., Haase, S., Michaud, K., & Hill, J.M. 1998, ApJS, 115.
- Snowden, S.L., McCammon, D., Burrows, D.N., & Mendenhall, J.A. 1994, ApJ, 424, 714.
- Stocke, J.T., Morris, S.L., Gioia, I.M., Maccacaro, T., Schild, R., Wolter, M., Fleming, T.A., & Henry, J.P. 1991, ApJS, 76, 813.
- Stark, A.A., Gammie, C.F., Wilson, R.W., Balley, J., Linke, R.A., Heiles, C., & Hurwit, M. 1992, ApJS, 79, 77.
- Struble, M.F., Rood, H.J. 1987, ApJ, 63, 543.
- Truemper, J. 1993, Science, 260, 1769.
- Tucker, W.H., Tananbaum, H., & Remillard, R.A. 1995, ApJ, 444, 532.
- Viana, P.T.P. & Liddle, A.R. 1999, MNRAS, 303, 535.
- Vikhlinin, A., McNamara, B.R., Forman, W., Jones, C., Quintana, H., & Hornstrup, A. 1998a, ApJ502, 558.
- Vikhlinin, A., McNamara, B.R., Forman, W., Jones, C., Quintana, H., & Hornstrup, A. 1998b, ApJ498, L21.
- Vikhlinin, A., McNamara, B.R., Hornstrup, A., Quintana, H., Forman, W., Jones, C., Way, M. 1999, ApJ520, L1.
- Zabludoff, A.I., Geller, M.J., Huchra, J.P., & Vogeley, M.S. 1993, AJ, 106, 1273.
- Zwicky, F., Herzog, E. & Wild, P. 1968, *Catalogue of galaxies and of clusters of galaxies*, Pasadena, CIT.

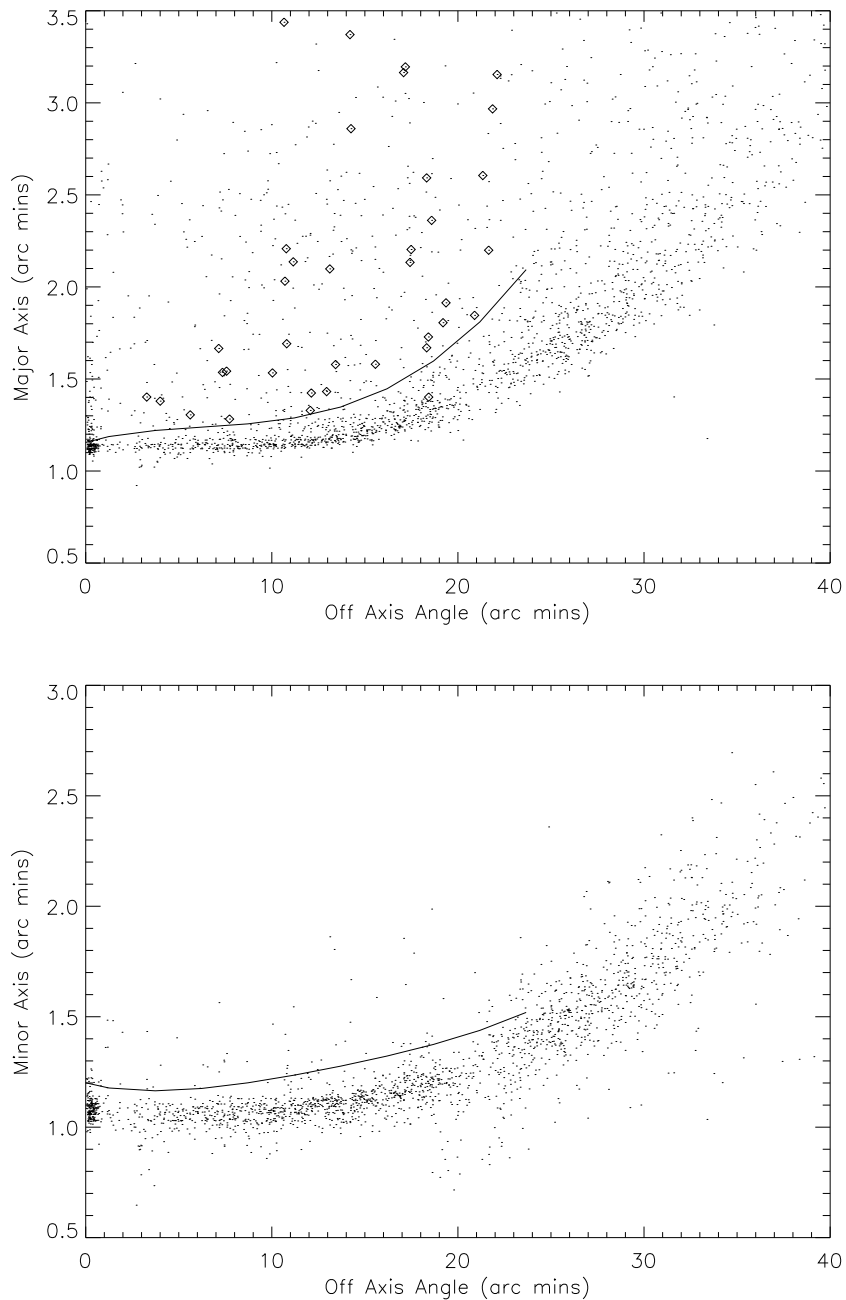


FIG. 1.— The distribution of major and minor axes for the 3,334 $S/N > 8$ sources in the Bright SHARC survey as a function of off-axis angle. The solid lines correspond to the fitted three-sigma extent curves; any sources falling above these lines are classified as extended. For illustration purposes, we have plotted, as open diamonds, the points corresponding to the thirty-seven Bright SHARC clusters on the major axis plot (the numerical values for these points can be found in Table 2).

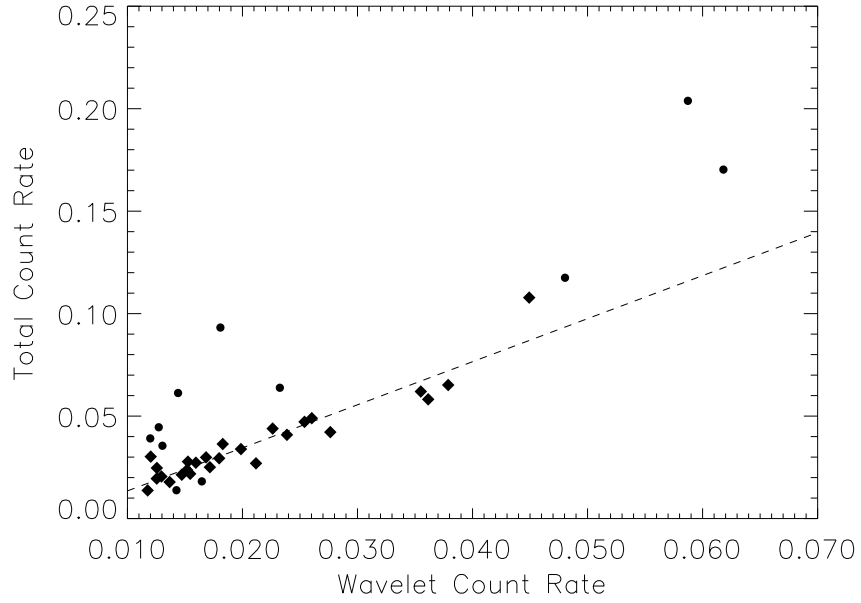


FIG. 2.— The wavelet count rate versus the total count rate for each of the thirty-seven clusters in the Bright SHARC sample. The low redshift ($z < 0.15$) clusters are indicated by circles. A least squares fit to the $z > 0.15$ clusters (diamonds) is shown by the dotted line (slope=2.1).

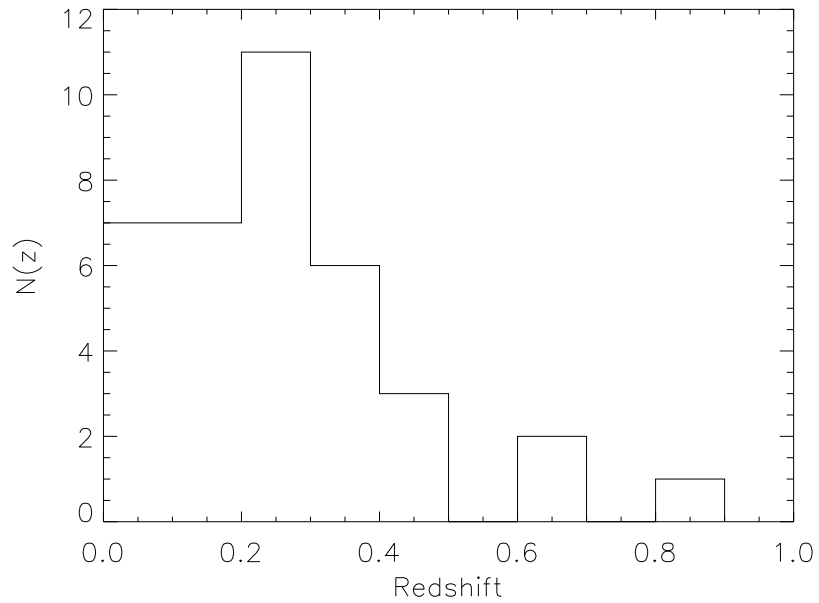


FIG. 3.— Redshift distribution of the thirty-seven clusters in the Bright SHARC.

TABLE 1
EXTENDED SOURCES IN THE BRIGHT SHARC SURVEY

Source (1)	RA (J2000) (2)	Dec (3)	cr_W (4)	Pointing (5)	ID (6)	ID code (7)	Notes (8)	Ref (9)
RX J0031.0–3547	00 31 03.0	–35 47 21.8	1.26	wp800387n00	Blend	X S N C	AGN, $z=0.25 + ?$	
RX J0031.9–3556	00 31 59.5	–35 56 12.1	1.19	wp800387n00	Blend	X S C	id pending	
RX J0058.0–2721	00 58 00.5	–27 21 29.3	1.18	rp701223n00	Blend	S N C	Mstar + ?	
RX J0117.6–2238	01 17 36.5	–22 38 13.5	1.25	rp100376n00	Cluster	S N C	A2894, $z=0.207$	
RX J0124.8+0932	01 24 48.2	+09 32 30.8	1.92	rp700976	Galaxy	N	NGC 524, $cz=2421$ km/s	1
RX J0152.7–1357	01 52 42.0	–13 57 52.9	1.71	rp600005n00	Cluster	S O C	$z=0.83$	2
RX J0209.4–1008	02 09 24.2	–10 08 04.2	1.34	rp800114n00	Galaxy	N	NGC0835, $z=0.0135$	3
RX J0209.9–1003	02 09 58.1	–10 03 19.2	1.47	rp800114n00	Blend	X S N C	QSO: MS0207.4, $z=1.97 + ?$	4
RX J0217.4–1800	02 17 26.1	–18 00 05.7	1.38	rp900352n00	Blend	S C	AGN, $z=0.345 + ?$	
RX J0221.1+1958	02 21 08.4	+19 58 25.9	1.54	wp900147	Cluster	S C	$z=0.45$	
RX J0223.4–0852	02 23 28.1	–08 52 14.3	1.20	rp800016n00	Cluster	S O N C	$z=0.163$	5
RX J0237.9–5224	02 37 59.1	–52 24 45.7	2.32	rp300201n00	Cluster	S O N C	A3038, $z=0.133$	6
RX J0250.0+1908	02 50 02.9	+19 08 29.4	1.42	rp700920	Cluster	S C	$z=0.12$	
RX J0256.5+0006	02 56 32.9	+00 06 11.6	3.61	rp701403n00	Cluster	S C	$z=0.36$	
RX J0318.2–0301	03 18 17.3	–03 01 21.1	1.33	wp800555n00	Blend	X S C	Cluster, $z=0.37 +$ AGN, $z=0.233$	
RX J0318.5–0302	03 18 33.3	–03 02 46.7	2.76	wp800555n00	Cluster	S C	$z=0.37$	
RX J0321.9–5119	03 21 57.0	–51 19 33.1	6.18	wp800371n00	Cluster	N	A3120, $z=0.0696$	7
RX J0324.6–5103	03 24 37.9	–51 03 52.1	1.32	wp800371n00	Blend	X D	Star:HD21360 + ?	
RX J0327.9+0233	03 27 54.3	+02 33 43.2	3.23	rp700099m01	Galaxy	N	UGC2748, $z=0.0302$	8
RX J0337.5–2518	03 37 34.2	–25 18 01.5	2.13	wp300079	Blend	X C	id pending	
RX J0340.1–4458	03 40 09.0	–44 58 48.2	1.24	rp900495n00	Pending	C		
RX J0359.1–5300	03 59 11.9	–53 00 56.2	1.51	rp800308	Blend	X D	2 stars	
RX J0414.0–1224	04 14 05.7	–12 24 24.9	2.50	rp900242n00	Blend	S N	AGN, $z=0.572 + ?$	9
RX J0415.7–5535	04 15 45.4	–55 35 31.0	1.20	wp600623n00	Galaxy	N	NGC1549, $cz=1197$ km/s	10
RX J0416.1–5546	04 16 10.3	–55 46 46.3	3.65	wp600623n00	Galaxy	N	NGC1553, $cz=1080$ km/s	11
RX J0420.9+1444	04 20 58.7	+14 44 07.7	2.83	wp200441	Blend	S C	AGN + ?	
RX J0421.2+1340	04 21 16.8	+13 40 14.8	1.32	rp200776n00	Blend	X S C	star + ?	
RX J0426.1+1655	04 26 07.3	+16 55 12.1	1.79	rp201369n00	Cluster	S C	$z=0.38$	
RX J0454.3–0239	04 54 19.6	–02 39 50.0	1.59	rp800229n00	Cluster	S C	$z=0.26$	
RX J0514.2–4826	05 14 16.7	–48 26 53.4	1.58	wp800368n00	Blend	X S C	AGN, $z=0.230 + ?$	
RX J0609.1–4854	06 09 06.5	–48 54 50.4	2.15	rp300111	Blend	D	star + ?	
RX J0849.1+3731	08 49 08.9	+37 31 47.9	1.29	rp700546n00	Cluster	S N C	A708, $z=0.23$	
RX J0853.6+1349	08 53 41.1	+13 49 29.5	1.17	rp700887n00	Blend	X D N	Star + Galaxy:MS0850.8, $z=0.194$	12
RX J0945.6–1434	09 45 40.4	–14 34 5.0	2.30	wp701458n00	Blend	X D S	AGN, $z \simeq 1.2 +$ star	
RX J0947.8+0741	09 47 50.5	+07 41 43.0	1.51	wp701587n00	Blend	S C	QSO, $z \simeq 0.63 + ?$	
RX J1010.2+5430	10 10 12.9	+54 30 09.6	1.41	wp900213	Group	N	V84 $z \simeq 0.045$	13
RX J1020.0+3915	10 20 02.4	+39 15 50.8	1.18	wp900528n00	Blend	X C	id pending	
RX J1024.3+6805	10 24 20.1	+68 05 05.1	2.60	wp800641n00	Cluster	N	A981, $z=0.201$	14
RX J1031.3–1433	10 31 23.3	–14 33 40.6	1.18	rp700461n00	Blend	D S	Star + ?	
RX J1113.8+4017	11 13 48.5	+40 17 18.3	1.44	rp700855n00	Cluster	N	A1203, $z=0.0795$	15
RX J1120.1+4318	11 20 07.5	+43 18 04.9	2.11	rp900383n00	Cluster	S C	$z=0.60$	
RX J1142.2+1026	11 42 16.7	+10 26 46.9	1.27	wp600420	Cluster	N	A1356, $z=0.0698$	16
RX J1143.7+5520	11 43 46.5	+55 20 13.6	1.98	rp600236n00	Blend	X D C	id pending	

TABLE 1
(CONTINUED)

Source (1)	RA (J2000) (2)	Dec (3)	cr_w (4)	Pointing (5)	ID (6)	ID code (7)	Notes (8)	Ref (9)
RX J1204.0+2807	12 04 03.6	+28 07 03.6	4.49	wp700232	Cluster	N	MS1201.5, $z=0.167$	17
RX J1204.1+2020	12 04 09.7	+20 20 40.5	2.04	rp800039	Galaxy	N	NGC4066, $z=0.024$	18
RX J1210.4+3929	12 10 25.9	+39 29 07.6	14.30	wp700277	Blend	N C	QSO:MS1207.9, $z=0.615 + ?$	19
RX J1211.1+3907	12 11 09.5	+39 07 44.4	2.14	rp600625n00	Blend	X D	Star + ?	
RX J1211.2+3911	12 11 14.5	+39 11 41.1	1.52	wp700277	Cluster	N	MS1208.7, $z=0.34$	20
RX J1220.3+7522	12 20 18.0	+75 22 10.2	4.65	rp700434	Galaxy	N	NGC4291, $z=0.059$	21
RX J1222.1+7526	12 22 06.9	+75 26 16.8	1.17	rp700434	Cluster	N	MS1219.9, $z=0.24$	22
RX J1222.5+2550	12 22 30.8	+25 50 26.7	36.93	wp200307	Blend	X D	2 Stars	
RX J1227.4+0849	12 27 27.6	+08 49 53.1	5.87	wp600587n00	Cluster	N	A1541, $z=0.0895$	23
RX J1232.8+2605	12 32 48.3	+26 05 39.0	1.82	rp600162	Cluster	S C	$z=0.22$	
RX J1241.5+3250	12 41 33.1	+32 50 22.9	2.38	rp600129a00	Cluster	S C	$z=0.39$	
RX J1244.1+1134	12 44 08.2	+11 34 16.8	1.16	rp600017	Blend	X C	id pending	
RX J1250.4+2530	12 50 26.1	+25 30 17.6	1.71	wp900212	Galaxy	N	NGC4725, $z=0.00402$	24
RX J1259.7-3236	12 59 45.4	-32 36 59.9	1.19	rp800384n00	Cluster	S C	$z=0.076$	
RX J1308.5+5342	13 08 32.6	+53 42 19.3	1.25	wp300394n00	Cluster	S C	$z=0.33$	
RX J1311.2+3228	13 11 12.3	+32 28 53.2	2.53	wp700216	Cluster	N C	MS1308.8, $z=0.245$	25
RX J1311.8+3227	13 11 49.8	+32 27 40.4	1.47	wp700216	Cluster	S C	$z=0.44$	
RX J1313.6-3250	13 13 41.0	-32 50 45.9	1.28	wp300219	Blend	X D	id pending	
RX J1334.3+5030	13 34 20.0	+50 30 54.2	1.36	rp800047	Cluster	S C	$z=0.62$	
RX J1343.7+5538	13 43 45.2	+55 38 20.3	1.80	rp700922n00	Cluster	N	A1783, $z=0.0766$	26
RX J1349.2-0712	13 49 12.3	-07 12 41.2	1.51	rp800637n00	Gal. pair	N	part of HCG67, $z=0.02406$	27
RX J1406.9+2834	14 06 55.1	+28 34 15.7	1.30	rp700061	Cluster	N S C	V154, $z=0.117$	
RX J1412.4+4355	14 12 29.8	+43 55 31.2	2.32	wp700248	Blend	X S N C	AGN, $z=0.095 + ?$	28
RX J1416.4+2315	14 16 26.6	+23 15 32.8	4.80	rp800401a01	Cluster	S C	$z=0.138$	
RX J1417.9+5417	14 17 57.5	+54 17 51.3	1.26	wp150046	Blend	O C	AGN + Mstar	29
RX J1418.5+2510	14 18 31.4	+25 10 45.8	3.78	wp150071	Cluster	S C	V159, $z=0.29$	
RX J1508.4+5537	15 08 24.6	+55 37 05.3	1.16	rp600119n00	Blend	D S C	Star + ?	
RX J1517.1+3140	15 17 08.4	+31 40 58.4	1.29	rp201018	Blend	X D S C	Star + ?	
RX J1524.6+0957	15 24 39.6	+09 57 44.8	1.64	rp701001n00	Cluster	S O C	V170, $z=0.078$	30
RX J1525.3+4201	15 25 23.3	+42 01 00.0	1.26	rp701405n00	Blend	N C	QSO, $z=1.189 + ?$	31
RX J1541.1+6626	15 41 10.3	+66 26 25.0	1.51	rp800511n00	Cluster	S C	$z=0.245$	
RX J1543.7+6627	15 43 42.7	+66 27 42.3	1.25	rp800511n00	Blend	S C	QSO, $z=1.4562 + ?$	
RX J1641.2+8233	16 41 13.9	+82 33 01.7	3.55	rp700098	Cluster	S N C	V183, $z=0.195$	32

TABLE 1
(CONTINUED)

Source (1)	RA (J2000) (2)	Dec (3)	cr_W (4)	Pointing (5)	ID (6)	ID code (7)	Notes (8)	Ref (9)
RX J1701.3+6414	17 01 22.5	+64 14 08.3	1.98	wp701457n00	Cluster	N S C	V190, $z=0.453$	33
RX J1705.6+6024	17 05 37.5	+60 24 11.0	1.46	rp701439n00	Pending	C		
RX J1726.2+0410	17 26 14.4	+04 10 23.8	1.98	rp200522n00	Blend	X D	Star + ?	
RX J1730.6+7422	17 30 37.6	+74 22 23.8	3.20	wp701200	Galaxy	N S C	NGC6414, $z=0.054$	
RX J1845.6+7956	18 45 41.3	+79 56 34.5	2.23	rp700058	Blend	X D	Star:HD175938 + ?	
RX J2109.7-1332	21 09 47.8	-13 32 24.2	1.38	rp201007n00	Blend	S C	QSO + ?	
RX J2202.8-5636	22 02 52.9	-56 36 08.3	1.63	rp200559n00	Blend	X D	id pending	
RX J2215.2-2944	22 15 16.4	-29 44 29.2	1.95	rp701390n00	Blend	N	QSO: HB89:2212-299, $z=2.7 + ?$	35
RX J2223.8-0206	22 23 48.8	-02 06 13.0	2.19	rp701018n00	Blend	S	AGN, $z=0.0558 + ?$	
RX J2236.0+3358	22 36 00.3	+33 58 24.0	3.18	wp800066	Group	N	Stef.Quintet, $z=0.0215$	36
RX J2237.0-1516	22 37 00.6	-15 16 08.0	1.68	wp201723n00	Cluster	S C	$z=0.299$	
RX J2258.1+2055	22 58 08.4	+20 55 15.0	2.26	rp201282n00	Cluster	S N C	Z2255.5, $z=0.288$	37
RX J2309.4-2713	23 09 27.9	-27 13 20.1	1.19	rp900323n00	Blend	S C	AGN, $z=0.25 + ?$	
RX J2311.4+1035	23 11 25.9	+10 35 06.7	3.52	rp100578n00	Blend	S C	AGN, $z=0.127 + ?$	
RX J2314.7+1915	23 14 44.0	+19 15 23.3	1.39	rp800488n00	Blend	S C	Cluster, $z=0.28 + Mstar$	
RX J2353.5-1524	23 53 31.5	-15 24 51.2	1.18	wp701501n00	Blend	S C	QSO + Mstar	

NOTES — Count rates (column 4) are quoted in units of 10^{-2} counts s^{-1} . ¹Redshift taken from De Vaucouleurs *et al.* (1991, D91 hereafter). ²Confirmation of redshift provided by Piero Rosati (private communication) and Ebeling *et al.* (1999). ³Redshift taken from D91. ⁴Redshift taken from Stocke *et al.* (1991, S91 hereafter). ^{5,6}Additional spectroscopy provided by Ian Del Antonio. ⁷Redshift taken from Abell, Corwin & Olowin (1989). ⁸Redshift taken from D91. ⁹Additional redshift information available in Perlman *et al.* (1998). ¹⁰Redshift taken from Longhetti *et al.* (1989). ¹¹Redshift taken from D91. ¹²Redshift taken from S91. ¹³Redshift taken from Carballo *et al.* (1995). ¹⁴Redshift taken from Huchra *et al.* (1989). ¹⁵Redshift taken from Slingsend *et al.* (1998). ¹⁶Redshift taken from Struble *et al.* (1987). ¹⁷Redshift taken from S91. ¹⁸Redshift taken from D91. ^{19,20}Redshift taken from S91. ²¹Redshift taken from D91. ²²Redshift taken from S91. ²³Redshift taken from Zabludoff *et al.* (1993). ²⁴Redshift taken from D91. ²⁵Redshift taken from S91. ²⁶Redshift taken from Struble *et al.* (1987) ²⁷Redshift taken from Fairall *et al.* (1992). ²⁸Additional redshift information available in Boyle *et al.* (1995). ²⁹Spectroscopy provided by Dave Turnshek and Eric Monier. ³⁰Spectroscopy provided by Ian Del Antonio. ³¹Redshift taken from Perlman *et al.* (1998). ³²Also known as EXSS 1646.5+8238 (Tucker *et al.* 1995). ³³Also known as “Cluster B” (Reimers *et al.* 1997). ^{34,35}Redshift taken from Hewitt & Burbidge (1993). ³⁶Redshift taken from Hickson *et al.* (1992). ³⁷Redshift taken from S91.

TABLE 2
BRIGHT SHARC CLUSTER CATALOG

Source (1)	Redshift (2)	nH (3)	Major (4)	Minor (5)	Offaxis (6)	cr_W (7)	cr_T (8)	δcr_T (9)	r_{80} (10)	f_{80} (11)	f_{-13} (12)	L_{44} (13)	T (14)	Notes (15)
RX J0117.6-2238	0.207	1.51	8.82	6.32	86.91	1.255	2.285	9.2%	18.36	0.943	2.594	0.4951	3	A2894
RX J0152.7-1357	0.83	1.42	11.4	4.99	57.22	1.716	2.440	5.6%	9.900	1.000	2.930	8.2604	9	
RX J0221.1+1958	0.45	9.30	6.70	5.47	73.54	1.545	2.211	6.2%	12.03	0.969	3.296	2.8661	6	
RX J0223.4-0852	0.163	3.18	8.86	4.98	43.25	1.202	3.036	7.7%	21.09	0.994	3.706	0.4350	3	(1)
RX J0237.9-5224	0.133	3.08	8.56	5.53	69.94	2.324	6.107	5.3%	24.63	0.906	7.495	0.5824	3	A3038
RX J0250.0+1908	0.12	9.40	13.5	5.92	57.00	1.426	1.576	15.3%	26.49	0.997	2.242	0.1443	2	
RX J0256.5+6.00	0.36	5.33	7.40	6.82	83.87	3.614	5.692	4.9%	13.44	0.998	7.549	4.1597	7	
RX J0318.5-0302	0.37	5.09	6.79	5.08	43.35	2.763	4.191	5.5%	12.85	1.000	5.587	3.2819	6	(2)
RX J0321.9-5119	0.0696	2.46	6.93	5.36	73.91	6.180	17.10	2.4%	40.23	0.916	20.72	0.4355	3	A3120 (3)
RX J0426.1+1655	0.38	16.4	5.23	4.55	22.54	1.797	2.948	6.3%	12.62	1.000	5.159	3.1969	6	
RX J0454.3-0239	0.26	5.24	10.4	5.92	85.65	1.594	2.732	8.0%	16.01	0.914	3.564	1.0634	4	(4)
RX J0849.1+3731	0.230	3.07	8.42	7.47	52.64	1.295	2.052	11.3%	16.84	0.991	2.525	0.5976	3	A708
RX J1024.3+6805	0.201	2.13	6.33	5.51	53.89	2.602	4.787	5.8%	18.38	0.991	5.699	1.0100	4	A981 (5)
RX J1113.8+4017	0.0795	1.80	12.6	4.36	88.73	1.440	5.879	6.1%	36.39	0.913	6.696	0.1866	2	A1203
RX J1120.1+4318	0.60	2.15	5.33	4.88	48.43	2.117	2.728	8.1%	10.63	1.000	3.285	5.0100	7	
RX J1142.2+1026	0.0698	3.33	6.15	5.88	40.27	1.272	4.245	10.8%	40.04	0.927	5.182	0.1110	2	A1356
RX J1204.0+2807	0.167	1.69	6.16	4.56	29.50	4.492	10.60	3.2%	20.93	0.997	12.38	1.4942	5	MS1201.5
RX J1211.2+3911	0.34	2.02	6.34	4.76	62.48	1.525	2.649	5.8%	13.52	0.988	3.163	1.5948	5	MS1208.7
RX J1222.1+7526	0.24	2.88	5.14	4.48	31.01	1.175	1.353	20.5%	16.28	1.000	1.630	0.4208	3	MS1219.9
RX J1227.4+0849	0.0895	1.70	9.48	7.97	74.61	5.872	19.75	2.5%	33.15	0.983	22.57	0.7876	3	A1541
RX J1232.8+2605	0.22	1.36	10.4	5.72	73.53	1.828	3.577	8.0%	17.47	0.932	4.136	0.8799	4	
RX J1241.5+3250	0.39	1.28	7.24	6.35	77.06	2.386	3.996	5.7%	12.98	0.999	4.748	3.0995	6	
RX J1259.7-3236	0.076	5.92	7.68	4.80	77.70	1.198	4.058	11.7%	37.59	0.884	5.222	0.1328	2	(6)
RX J1308.5+5342	0.33	1.59	8.57	6.20	44.76	1.254	1.732	10.7%	13.62	1.000	1.978	0.9579	4	
RX J1311.2+3228	0.245	1.08	5.71	5.19	48.66	2.539	4.647	5.7%	16.11	1.000	5.376	1.4223	4	MS1308.8
RX J1311.8+3227	0.43	1.08	5.62	5.52	73.97	1.472	2.029	9.4%	12.22	0.913	2.375	1.9237	5	
RX J1334.3+5030	0.62	1.08	8.84	5.04	70.18	1.366	1.810	8.4%	10.76	0.990	2.091	3.4606	6	(7)
RX J1343.7+5538	0.0766	1.05	12.8	6.60	68.94	1.808	9.228	4.9%	37.31	0.946	10.32	0.2668	2	A1783
RX J1406.9+2834	0.117	1.40	6.68	5.01	28.69	1.304	3.625	7.3%	26.93	0.987	4.085	0.2497	2	V154
RX J1416.4+2315	0.138	2.04	13.7	4.87	42.77	4.804	11.18	4.6%	23.86	0.989	13.33	1.1066	4	(8)
RX J1418.5+2510	0.29	1.78	6.19	5.35	30.37	3.788	6.549	3.8%	14.62	1.000	7.655	2.7618	6	V159
RX J1524.6+0957	0.078	2.88	5.53	5.14	16.07	1.646	2.236	29.8%	36.70	0.914	2.371	0.0649	1	V170
RX J1541.1+6626	0.245	2.90	8.15	5.70	42.96	1.517	2.356	7.7%	16.11	0.999	2.814	0.7578	3	(9)
RX J1641.2+8233	0.195	5.51	12.7	7.44	68.56	3.550	6.227	5.2%	18.87	0.993	8.128	1.3550	4	V183
RX J1701.3+6414	0.453	2.51	5.62	4.71	13.16	1.986	3.302	4.7%	11.62	0.997	3.965	3.4935	6	V190
RX J2237.0-1516	0.299	3.90	11.9	5.65	87.75	1.683	2.723	7.7%	14.91	0.990	3.413	1.3525	4	
RX J2258.1+2055	0.288	4.91	5.74	4.81	51.96	2.262	4.428	6.1%	14.76	0.997	5.694	2.0550	5	Z2255.5

NOTES — Count rates (columns 4 & 5) are quoted in units of 10^{-2} counts s^{-1} . ¹RX J0223.4 ($z=0.163$) was detected in pointing rp800016n00, the central target of which was a wide angle radio (WAR) source. The cluster hosting this WAR source has a redshift of $z=0.41$ (Nichol *et al.* 1994a). The redshift separation of the two clusters is $\delta z \simeq 0.247$. ²RX J0318.5 ($z=0.37$) was detected in wp800555n00 which was pointed, accidentally, $\sim 40^\circ$ away in declination away from the listed target, A3112, which lies at 03:17:56-44:14:17 (Ebeling *et al.* 1996). ³RX J0321.9 (A3120, $z=0.0696$) was detected in wp800371n00, the central target of which was a Couch *et al.* (1991) cluster at $z=0.49$. The redshift separation of the two clusters is $\delta z=0.42$. ⁴RX J0454.3 ($z=0.26$) was detected in rp800229n00, the central target of which was cluster MS0451.6 ($z=0.55$, Gioia & Luppino 1994). The redshift separation of the two clusters is $\delta z=0.29$. ⁵RX J1024.3 (A981, $z=0.201$) was detected in wp800641, the central target of which was cluster A998 ($z=0.202$, Huchra *et al.* 1989). The redshift separation of the two clusters is $\delta z=0.001$. ⁶RX J1259.7 ($z=0.076$) was detected in rp800384n00, the central target of which was cluster A3537 ($cz=5007$ km/s, Abell, Corwin & Olowin 1989). The redshift separation of the two clusters is $\delta z=0.059$. ⁷RX J1334.3 ($z=0.62$) was detected in rp800047, the central target of which was cluster A1758 ($z=0.2792$, Allen *et al.* 1992). The redshift separation of the two clusters is $\delta z=0.34$. ⁸RX J1416.4 ($z=0.138$) was detected in rp800401a01, the central target of which was galaxy 4C23.37 ($cz=154$ km/s, De Vaucouleurs *et al.* 1991). The redshift separation of the two clusters is $\delta z=0.137$. ⁹ RX J1541.1 ($z=0.245$) was detected in rp800511n00, the central target of which was A2125 ($z=0.2465$, Struble *et al.* 1987). The redshift separation of the two clusters is $\delta z=0.0015$.

TABLE 3
COMPARISON OF BRIGHT SHARC AND V98 FLUX MEASUREMENTS

Bright SHARC ID.	V98 ID.	Redshift	f_{-13}	Ratio ¹	Ratio ²
RX J0237.9-5224	V28	0.1330	7.495	1.16	1.06
RX J0849.1+3731	V62	0.2300	2.525	1.72	1.48
RX J1204.0+2807	V112	0.1670	12.38	1.21	0.91
RX J1211.2+3911	V115	0.3400	3.163	1.19	0.83
RX J1308.5+5342	V132	0.3300	1.978	1.15	0.91
RX J1406.9+2834	V154	0.1170	4.085	1.58	1.22
RX J1418.5+2510	V159	0.2900	7.655	1.01	0.95
RX J1524.6+0957	V170	0.0780	2.371	0.78	0.83
RX J1641.2+8233	V183	0.1950	8.128	1.01	1.04
RX J1701.3+6414	V190	0.4530	3.965	1.03	0.92
RX J2258.1+2055	V213	0.2880	5.694	1.13	0.93
Average				1.18	1.01

NOTES — ¹Ratios of the Bright SHARC fluxes (column 4) to the Vikhlinin *et al.* (1998a V98) fluxes. ²Ratios of the re-calculated Bright SHARC fluxes to the V98 fluxes, see §7.1 for details.